UC Santa Cruz

UC Santa Cruz Previously Published Works

Title

Measurement of the Heme Affinity for Yeast Dap1p, and Its Importance in Cellular Function †

Permalink

https://escholarship.org/uc/item/90c6q43k

Journal

Biochemistry, 46(50)

ISSN

0006-2960

Authors

Thompson, Alisha M
Reddi, Amit R
Shi, Xiaoli
et al.

Publication Date

2007-12-01

DOI

10.1021/bi7013739

Copyright Information

This work is made available under the terms of a Creative Commons Attribution License, available at https://creativecommons.org/licenses/by/4.0/

Peer reviewed

eScholarship.org Powered by the California Digital Library
University of California

NIH Public Access
Author Manuscript
Biochemistry. Author manuscript; available in PMC 2009 April 16.

Published in final edited form as:
Biochemistry. 2007 December 18; 46(50): 14629–14637. doi:10.1021/bi7013739.

Determination of the Heme Affinity for Yeast Dap1p, and its Importance in Cellular Function†

Alisha M. Thompson‡, **Amit R. Reddi**§, **Xiaoli Shi**&, **Robert A. Goldbeck**‡, **Pierre Moënne-Loccoz**⊥, **Brian R. Gibney**§, and **Theodore R. Holman**‡,*

‡*Department of Chemistry and Biochemistry, University of California, Santa Cruz, CA, 95064, USA*

§*Department of Chemistry, Columbia University, 3000 Broadway, MC 3121, New York, New York, 10027, USA*

⊥*Department of Environmental & Biomolecular Systems, OGI School of Science & Engineering, Oregon Health & Science University, 20,000 NW Walker Road, Beaverton, Oregon 97006, USA*

Abstract

Current studies on the Saccharomyces cerevisiae protein Dap1p have demonstrated a heme related function within the ergosterol biosynthetic pathway. Here we present data to further the understanding of the role of heme in the proper biological functioning of Dap1p in cellular processes. Firstly, we examined the role of Dap1p in stabilizing the P_{450} enzyme, Erg11p, a key protein involved with facilitating ergosterol biosynthesis. Our data indicates that the absence of Dap1p does not affect Erg11p mRNA or protein expression levels, nor the protein degradation rates. Secondly, in order to probe the role of heme in the biological functioning of Dap1p, we measured ferric and ferrous heme binding affinities for Dap1p and the mutant $Dap1p^{Y138F}$, as well as equilibrium midpoint reduction potentials of the Fe(III)/Fe(II) couples. Our results show that both wild-type and mutant proteins bind heme in a 1:1 fashion, possessing tight ferric heme affinities, K_D values of 400 pM and 200 nM, respectively, but exhibiting weak ferrous affinities, 2 μM and 10 μM respectively. Additionally, the measured reduction potential of Dap1p, which was found to be 307 mV, is similar to that of other mono-tyrosinate hemoproteins. Although the weaker affinity of $Dap1p^{Y138F}$ for ferric heme lowers the production of ergosterol with respect to wild-type Dap1p, it is still sufficient to rescue the growth sensitivity of dap1Δ to fluconazole and MMS, suggesting that the activity of Dap1p is directly related to its ability to bind heme.

The yeast protein, Dap1p, belongs to a highly conserved and ubiquitous protein family known as membrane associated progesterone receptors, MAPR's. The first characterized member of this family was found in porcine liver tissues and was identified by its ability to bind progesterone(1–3). Homologous members of this family have been identified, via sequence alignments, in all eukaryotes, from protozoans to humans. They share a conserved cytochrome b_5 heme binding motif (4), although, the protein sequences lack the two histidines required for cytochrome b_5 binding of heme. Nevertheless, within the last five years, evidence has been mounting towards a biological role for heme binding with several of the well characterized MAPR's, including Dap1p (5–9).

*To whom the correspondence should be sent. E-mail: tholman@chemistry.ucsc.edu.
&*Current Address:* Department of Radiation Oncology, Stanford University, Palo Alto, CA, 94305, USA

†This research was supported by NIH Grant GM56062-06 (T.R.H.), the Roche Foundation for Anemia Research (T.R.H.), NIH Grant EB02056 (R.A.G.) and the American Heart Association Grant-in-Aid (0755879T) (B.R.G.).

NIH-PA Author Manuscript
NIH-PA Author Manuscript
NIH-PA Author Manuscript

NIH-PA Author Manuscript

NIH-PA Author Manuscript

NIH-PA Author Manuscript

Yeast Dap1p was first characterized in a deletion strain, *dap1Δ*, by its sensitivity to methyl methanesulfonate (MMS), a DNA damaging agent, and fluconazole/itraconazole, Erg11p sterol synthesis inhibitors (10). *Dap1Δ* strains were later shown to be rescued from the MMS sensitivity by the presence of hemin in the media, both in growth and sterol production (7). Mallory, et al. also demonstrated that over-expression of Erg11p in *dap1Δ* lowered the sensitivity against itraconazole. Although, *dap1Δ* did not affect mRNA levels of Erg11p, Mallory did report lowered protein levels of Erg11p, suggesting a protein regulatory function for Dap1p, possibly as a heme chaperone (7). It was also reported at this time that a Dap1p fusion protein bound heme, although its heme ligation was unknown. The heme binding of Dap1p was further characterized by our group as a penta-coordinate, ferric heme, with Tyr138 as the axial ligand (6). Recently, Hughes et al, reported that Dap1p bound Erg11p in a 1:1 ratio and that heme binding by Dap1p was important for maintaining sterol production, by comparing the sterol profile of wild-type, *dap1Δ*, and Dap1p^{Y138F} strains (8). Hughes et al. also demonstrated that the protein level of the human homologue of Erg11p, Cyp51A1, was not affected by the loss of the human homologue of Dap1p, PGRMC1, supporting their hypothesis that MAPR's activate P_{450} cytochromes through a protein-protein interaction and not by chaperoning heme, contrary to past hypotheses (5–7). For these reasons, we set out in this study to further characterize the cellular and biochemical properties of Dap1p in an attempt to understand its role in yeast biology in more detail.

Methods and Materials

Source of Materials

Restriction endonucleases were obtained from New England BioLabs (Beverly, MA). All other reagents were reagent grade or better and were used without further purification.

Plasmids, Strains, and Growth Conditions

The *E.coli* protein expression plasmids for Dap1p and Dap1p mutants were constructed as previously reported (6). Briefly, PCR amplified DAP1 gene from yeast genomic DNA was cloned into the pET28a vector (Novagen) generating the pET28a_DAP1 plasmid. All mutants were subsequently created by site-directed mutagenesis, using a Quikchange kit (Stratagene), and verified by DNA sequencing.

Yeast vector pRS313_DAP1 containing the native DAP1 promoter was constructed by PCR amplifying the DAP1 open reading frame along with 340 bps of promoter sequence and 254 bps of 3' UTR, cloned into pCR2.1-TOPO (Invitrogen) and sub-cloned into SpeI/Xho I sites of the low-copy vector pRS313. Dap1p^{D91G} was made by site directed mutagenesis on both the pRS313_DAP1 and pET28a_DAP1 plasmids. Wild-type (BY4741) and isogenic *dap1Δ* (BY4741-dap1::KanMX) were transformed with pRS313, pRS313_DAP1, or pRS313_DAP1^{Y138F} plasmid and grown on selective media.

pRS413GAL_ERG11-HA plasmid was created as follows: EcoR I (5') / Xho I (3') fragment containing the *ERG11* open reading frame plus 3HA tag right before the stop codon was generated by PCR from genomic DNA of BY4741 strain and cloned into the EcoR I and Xho I sites of *pRS413GAL* vector.

pRS303_ERG11-HA was created by sub-cloning ~1.3 Kb Xba I / Xho I C-terminal fragment of *ERG11* from *pRS413GAL_ERG11-HA* plasmid into a *pRS303* vector. *pRS303_ERG11-HA* was linearized by cutting with the unique BspM I and Pflm I within the C-terminal of ERG11 ORF and transformed into BY4741 wild-type and *dap1Δ* strains to generate strains genomically tagged *ERG11-HA*. The integration was confirmed by PCR. The above ERG11-

NIH-PA Author Manuscript

NIH-PA Author Manuscript

NIH-PA Author Manuscript

HA tagged strains were grown overnight, diluted, grown in SD-His medium for 4 hr and then harvested for qRT-PCR and western blotting, respectively.

Quantitative RT-PCR

Early -log phase cells, treated with or without 25 μM hemin were harvested and the total RNA was extracted by Qiagen RNeasy mini Kit. Contaminating DNA was removed from 16 μl of RNA extract by the addition of 2 μl 10X reaction buffer and 2 μl of DNase (Promega RQ1 DNase) and incubating for 30 min at 37°C. Reactions were terminated by adding 2 μl of Stop Buffer and heating for 10 min at 65°C. cDNA was synthesized using Applied Biosystem TaqMan reverse transcription kit by the following modified protocol. Each 20 μl reaction consisted of: 2 μl 10X TaqMan RT Buffer, 4.4 μl 25 mM $MgCl_2$, 4 μl dNTP mix, 1 μl Random Hexamers, 0.4 μl RNase Inhibitor, 0.6 μl Multiscribe Reverse Transcriptase (50 U/μl), 7.6 μl DNase-treated RNA sample (1 μg total RNA). Reactions were incubated at 25°C for 10 min, 48°C for 30 min, followed by heat inactivation at 95°C for 5 min. Prior to quantitative PCR, cDNAs were diluted 1/4 in nuclease-free water.

The following primers were used for real time PCR analyses:

ERG11(f): 5’ TTCCGTCGGTGAAGAAGTCGATTACG 3’,

ERG11(r): 5’ ACATCTGTGTCTACCACCACCGAAAG 3’,

TBP(f): 5’ CGGTTCGTGTGACGTTAAATTCC 3’,

TBP(r): 5’ GCACAGGGTATATAGCTTCAAAAGC 3’

. PCR reactions consisted of 4 μl diluted template (cDNA, standard genomic DNA, or water), 20 μl 2X SybrGreen Taq Mix (Applied Biosystems), 300 nM each primer, and nuclease-free water to make a final volume of 40 μl. PCR was carried out using a MJ Research Opticon 2 in duplicate for triplicate cDNA samples and primer sets. Thermocycle profile was as follows: 95°C for 10 min, 40 cycles of 95°C 30 sec and 60°C 1 min, with a final denaturation cycle to examine the DNA melting curves of PCR products.

The cycle thresholds (C(t)) were calculated for samples and genomic DNA standards. For each transcript, the C(t) value was converted to a nanogram genomic DNA equivalent by comparing the C(t) of an unknown to standard curves prepared from genomic DNA of strain BY4741(1, 0.1, 0.01, 0.001 ng). Slopes for *ERG11* and *TBP* standard curves ranged from 3.3–4.3 and were linear with R^2 of 0.999. Expression was calculated by normalizing the nanogram value for *ERG11* to the nanogram value of *TBP*.

Western blotting (determination of protein half-life)

Wild-type and isogenic *dap1Δ* yeast strains transformed with *pRS413GAL_ERG11-HA* were grown overnight in SD-His medium containing 2 % raffinose, inoculated in the same media and grown for 4 h. Galactose (0.5%) was added to the SD-His media (2% raffinose) to induce Erg11p protein expression. After 4 h of induction, cells were centrifuged and resuspended in SD-His containing 2% glucose to stop the induction. Aliquots at 0, 60, 120, and 240 mins, after stopping induction, were removed for immunoblot analysis. Protein extracts, with the same amount of OD_{600} units by NaOH/ β-mercaptoethanol method, were loaded onto 10 % SDS-PAGE and separated by electrophoresis. After transferring, the blot was incubated with a primary rabbit anti-HA antibody Y11 (Santa Cruz Biotech) and HRP-conjugated secondary goat anti–rabbit IgG (Santa Cruz Biotech.), developed by ECL, and recorded on ECL Hyper film (Amersham). The same blot was subsequently incubated with a primary mouse anti-yeast 3-phosphoglycerate kinase (PGK) monoclonal antibody (Molecular Probes Invitrogen) and a HRP- conjugated secondary goat anti-mouse IgG (Santa Cruz Biotech.) as a loading control (11).

NIH-PA Author Manuscript

NIH-PA Author Manuscript

NIH-PA Author Manuscript

Growth phenotype in Fluconazole or MMS media

The early log-phase cells (OD_{600} = 0.2) were serially diluted 10-fold with water and spotted into selective SD media containing either fluconazole or MMS. The plates were incubated at 30°C for 3 days and photographed.

Purification of Proteins

Purification and expression of Dap1p and Dap1p^{Y138F} was from *E.coli* BL21(DE3) cells and has been previously reported (6). Briefly, single colonies of freshly transformed cells were grown in LB broth containing 25 μg/ml of kanamycin (FisherBiotech) at 37°C and 200 rpm until an OD_{600} of 0.6 was attained. Cultures were then induced with 0.5 mM IPTG and grown overnight at 20°C and 100 rpm. Cell lysates were precipitated with ammonium sulfate, the 10–40% fraction was passed over a methyl hydrophobic interaction column, and the cleanest protein fractions were passed over a size exclusion column. Fractions of greater than 90% purity, as determined by PAGE, were collected, concentrated, and stored at −80°C in 5% glycerol.

Circular Dichroism

Purified protein samples, 70–90 μM, were measured in a 0.1 mm cuvette on a AVIV Model 60DS, from 190–240 nM, in 0.5 nm increments. The average of five spectra were integrated and measurements of percent alpha-helicity were based on the absorbance at θ_{222} nm and calculated with the equation $-\theta_{222}/33{,}000$= % alpha-helicity (12).

Measurement of Protein and Heme Extinction Coefficients

Heme content was measured by both ICP-MS analysis and pyridine hemochrome method (6, 13). Protein concentrations were measured by amino acid analysis, AAA, (UC Davis) and Bradford Assay (BioRad). Myoglobin was used as a standard due to its similarity in size to Dap1p and its heme binding. The protein extinction coefficient was back calculated from amino acid analysis by the summation of all amino acids measured against an internal standard, norleucine; a molar protein concentration could then be compared to the electronic spectra (http://msf.ucdavis.edu/calculations.html). The contribution of the heme to the UV-Vis absorption at 278 nm was determined by titration of heme into Dap1p and relating it to the Soret band.

Heme Reconstitution

A freshly prepared 100 × Hemin stock solution in 0.1M NaOH and 50% dimethyl sulfoxide, was used to add 1.5–2 fold excess heme to Dap1p and Dap1p^{Y138F} protein solutions. Protein and heme were left over night to equilibrate, and then washed three times with buffer in 10 kDa centricons for removal of unbound heme. Heme concentration was measured by ICP-MS, and protein concentration by UV-Vis absorption and Bradford.

Determination of Binding Constants

The heme binding affinity of Dap1p was measured using two competition binding methods. First, direct titration of horse skeletal muscle (HSM) apo-myoglobin into as-isolated, ferric Dap1p, with ~30% heme bound, was used to estimate the ferric heme K_D value of Dap1p. Singular value decomposition of the UV-Vis spectra coupled with fitting to a competition binding model was used to determine the ferric K_D^{comp} value (14). The K_D value of Dap1p was estimated based on the experimentally derived K_D^{comp} value and the K_D value of HSM myoglobin, estimated to be similar to the 28 fM ferric heme K_D value of sperm whale myoglobin (calculations and methods outlined in the supplemental data) (15). Due to the kinetic

NIH-PA Author Manuscript

NIH-PA Author Manuscript

NIH-PA Author Manuscript

trapping of ferrous heme by myoglobin and the lack of a measured ferrous heme K_D value, this could not be used to determine the ferrous K_D value of Dap1p (16).

In order to determine more accurate ferric and ferrous K_D values for Dap1p, direct competition titration experiments were performed using a synthetic heme protein maquette, $[\Delta 7\text{-His}]_2$, whose ferric and ferrous K_D values are well-described between pH 5.0 and 9.0. At pH 8.0, $[\Delta 7\text{-His}]_2$ possesses a ferric heme K_D value of 160 pM and a ferrous heme K_D value 40 nM and is kinetically competent for heme transfer experiments (17). In the ferric heme state, apo-$[\Delta 7\text{-His}]_2$ was titrated into a solution of 15 μm Dap1p containing 2.8 μM bound heme which resulted in a shift in the Soret band maximum from 398 nm to 412 nm. Heme transfer was evidenced by the increase in the intensity of the Soret at 412 nm which was monitored after an hour equilibration time.

For ferrous heme equilibrium measurements, apo-$[\Delta 7\text{-His}]_2$ was titrated into a solution of 10.6 μM Dap1p containing 2 μM bound heme under anaerobic conditions and maintained under a reducing redox environment, with the addition of a slight excess of sodium dithionite. Over the hour equilibration time the Soret band shifts from 422 nm to 427 nm, indicative of heme transfer to the synthetic protein. The equilibrium concentrations of holo-Dap1p and holo-$[\Delta 7\text{-His}]_2$ were calculated based on the intensity at 427 nm.

The heme binding stoichiometry and heme affinity of $Dap1p^{Y138F}$ was determined by direct titration of ferric or ferrous heme, the latter under reducing, anaerobic conditions with a slight excess of sodium dithionite. The affinity of $Dap1p^{Y138F}$ for ferric heme was determined by measuring the increase in absorbance at 398 nm and fitting the data to a 1:1 heme:protein binding equilibrium. The affinity of $Dap1p^{Y138F}$ for ferrous heme was determined in an analogous fashion using the increase in absorbance at 422 nm.

Resonance Raman Spectroscopy

Typical enzyme concentration for the resonance Raman (RR) experiments were ~ 150 μM in 25 mM HEPES (pH 7.4) buffer solution. Reduction to the ferrous state was achieved by adding microliter aliquots of a 10 mM sodium dithionite solution to argon-purged samples in the Raman capillary. The carbonyl complex was formed by direct injection of CO (Airgas) in the Raman capillary through a septum. RR spectra were obtained on a custom McPherson 2061/207 spectrometer (0.67 m with variable gratings) equipped with a Princeton instruments liquid N_2-cooled CCD detector (LN-1100PB) and Kaiser Optical supernotch filters. A krypton laser (Innova 302, Coherent) and an argon laser (Innova 90C, Coherent) were used for the 413 and 514.5 nm excitations, respectively. Spectra were collected in a 90° geometry on samples at room temperature with a collection time of a few minutes. Frequencies were calibrated relative to indene and CCl_4 and are accurate to ± 1 cm^{-1}. Sample heating and photochemistry was prevented by keeping the laser power below 5 mW and mounting the samples on reciprocating translation stage. Optical spectra were obtained before and after the RR experiments directly in the Raman capillaries and confirmed the integrity of the samples after laser illumination.

Determination of Heme Reduction Potential of Dap1p

Chemical redox titrations were performed in an anaerobic cuvette equipped with a platinum working and a calomel reference electrode at 22°C (18). Ambient potentials (measured against the standard hydrogen electrode) were adjusted by addition of aliquots (<1 μL) of sodium dithionite or potassium ferricyanide. Titrations were performed in 20 mM potassium phosphate, 100 mM KCl, pH 8.0. Electrode-solution mediation was facilitated by the following mediators at 10 μM concentration: methyl viologen, benzyl viologen, anthroquinone-2-sulfonate, anthroquinone-2,6-disulfonate, 2-hydroxy-1,4-naphthoquinone, duroquinone, 5-hydroxy-1,4-naphthoquinone, 1,4-naphthoquinone, phenazine ethosulfate, and phenazine

NIH-PA Author Manuscript

NIH-PA Author Manuscript

NIH-PA Author Manuscript

methosulfate. After equilibration at each potential, the optical spectrum was recorded. Heme reduction was followed by the increase in the Soret-band absorption (422 nm) relative to a baseline wavelength (750 nm). Spectral intensity was plotted against potential and the data were fit to a single Nernst equation with n = 1.0 (fixed).

Results

mRNA and Protein Expression

mRNA expression levels of ERG11, measured by quantitative real-time PCR in wild-type and *dap1Δ* strains, were found to be unaffected by the absence of Dap1p, as previously reported (7). Additionally, mRNA expression levels were unaffected by the addition of hemin (Figure 1). Protein levels of genomically tagged Erg11p-HA were measured from wild-type and *dap1Δ* yeast strains, standardized to the house keeping protein, PGK. Contrary to previously published results, Erg11p protein levels were found to be unaffected by the absence of Dap1p, relative to PKG (7) (Figure 1). Erg11p protein degradation levels were monitored by western blot and standardized to PKG protein levels at 0, 1, 2, and 4 hours after the induction/repression. The half-life ($t_{1/2}$) of Erg11p was plotted and calculated to be 40 minutes and 38 minutes in wild-type and *dap1Δ* strains, respectively (Figure 2).

Sensitivity to Fluconazole and MMS

Dap1p, Dap1p^{Y138F}, and Dap1p^{D91G} were transformed into wild-type and *dap1Δ* yeast strains and plated on selective media. The *dap1Δ* strain exhibits a growth sensitivity to media containing fluconazole or MMS which can be recovered by native expression of Dap1p but not by Dap1p^{D91G} (data not shown), as previously reported by Mallory, et al (7). However, Dap1p^{Y138F} can rescue the growth sensitivity for both fluconazole and MMS to wild-type growth, as shown in Figure 3.

Expression and Purification

Dap1p and Dap1p^{Y138F} were both expressed in *E.coli* at high levels, as previously reported (6). Attempts to purify a soluble form of untagged or his-tagged Dap1p^{D91G} were unsuccessful due to inclusion bodies, despite high levels of expression.

Circular Dichroism

Circular dichroism was used to measure percent α-helicity to insure Dap1p and Dap1p^{Y138F} were not grossly misfolded. Dap1p and Dap1p^{Y138F} were found to have 48% and 40% α-helicity respectively, based on θ_{222} values of 13,252 and 15,858. These numbers are comparable to the NMR structure of the plant homologue, At2g24940.1 (PDB = 1T0G), which indicates ~31% alpha-helicity. The difference may be accounted for by both the smaller size of At2g24940.1 (101 amino acids compared to 152 for Dap1p) and the lack of bound heme from its *in vitro* expression (19).

Determination of the Heme Extinction Coefficient

Quantification of heme concentration is typically done by measurement of the ferrous pyridine heme complex (13); however we have found the standard extinction coefficients associated with this method vary with both buffer and pH changes. Instead, we used ICP-MS to determine heme concentration based on iron analysis. From multiple protein preparations, we averaged an extinction coefficient of 96,800 ± 6,000 M^{-1} cm^{-1} for Dap1p, which is within error of our previously reported value of 99,000 M^{-1} cm^{-1}(6). Based on this value, a small feature for Dap1p^{Y138F}, as purified, is noted at 399 nm, corresponding to less then 2% heme bound (Figure 4).

NIH-PA Author Manuscript

NIH-PA Author Manuscript

NIH-PA Author Manuscript

Determination of Protein Extinction Coefficient

The protein extinction coefficient for Dap1p^{Y138F} was measured by both amino acid analysis and Bradford assay. The average ε_{278} for Dap1p ^{Y138F} (<2% heme bound) was measured as 17,000 ± 3,500 M^{-1} cm^{-1} , which is within the range of the predicted extinction coefficient of 15,500 M^{-1} cm^{-1} (ExPASy ProtParam tool). Determination of the ε_{278} for wild-type Dap1p is complicated by the additional heme absorption at 278 nm. To account for this variable we assumed the protein extinction coefficient for wild-type to be similar to that of the mutant Dap1p^{Y138F} (collaborated with the predicted value of 17,000 M^{-1} cm^{-1}, ExPASy ProtParam tool) and solved for the additional heme extinction coefficient at 278 nm. Based on a titration of heme into a solution of Dap1p, we compared the change at 399 and 278 nm, and using our known heme extinction coefficient of 96,800 ± 6,000 M^{-1} cm^{-1}, have found the heme extinction coefficient at 278 nm to be approximately 22,500 ± 3770 M^{-1} cm^{-1}.

Heme Binding Constants

Removal of heme from Dap1p was hampered by the fact that standard methods of heme extraction denatured the protein (20,21). Therefore, to measure the K_D, we switched to a competitive binding method using HSM apo-myoglobin and a 30% heme-loaded Dap1p sample. This method was used to determine an initial ferric heme dissociation constant of approximately 100 fM for Dap1p, assuming the HSM myoglobin had the same K_D value as that of sperm whale myoglobin, *i.e.* 28 fM (Supplemental data, Figure S1) (16).

In order to obtain a more accurate K_D values in both oxidation states, we utilized the synthetic heme protein maquette, $[\Delta 7\text{-His}]_2$, which has well determined K_D values in both the ferric and ferrous heme states (22). As previously reported, $[\Delta 7\text{-His}]_2$ has a ferric K_D value 160 pM and a ferrous heme K_D value 40 nM at pH 8.0 (17). Upon titration of apo-$[\Delta 7\text{-His}]_2$ to a solution of as-isolated Dap1p, under ferric and ferrous conditions, K_{comp} values are measured as 2.5 ± 1.0 and 35 ± 15, respectively, and with 1:1 heme to protein ratios in both cases. The ferric heme dissociation constant value for Dap1p was then calculated to be 400 ± 200 pM, and the ferrous dissociation constant value is 2 ± 1 μM (Figure 5).

For the mutant Dap1p^{Y138F}, direct titration of heme was possible due to the low initial concentration of heme (<2%) from purification and a weaker affinity for heme. A protein to heme binding ratio of 1:1 is observed by direct titration and ferric and ferrous heme dissociation constants for Dap1p^{Y138F} were measured as 200 ± 100 nM and 10 ± 5 μM, respectively (Figure 6).

RR characterization of Dap1p

The high-frequency region of the RR spectra of Dap1p in the ferric, ferrous, and ferrous-CO state are shown in Figure 7. The ferric protein displays fully symmetric porphyrin modes ν_4 and ν_3 at 1373 and 1489 cm^{-1}, respectively. These frequencies are characteristic of a 5-coordinate high-spin ferric heme (23). In porphyrins bound to a proximal histidine, the ν_4 mode dominates the high-frequency spectra, but in Dap1p, as in other hemoproteins lacking a proximal histidine, the ν_4 and ν_3 modes have comparable intensities (24,25). Attempts to confirm the iron(III) ligation to a tyrosine with RR experiments using a 514.5-nm excitation were inconclusive (data not shown). Upon reduction with dithionite, the ν_4 oxidation-state marker band shifts to 1360 cm^{-1} while the ν_3 and ν_{10} at 1471 and 1604 cm^{-1}, respectively, are indicative of a 5-coordinate high-spin configuration (Figure 7). Binding of CO up-shifts these frequencies (ν_4 at 1374, ν_3 at 1503, and ν_{10} at 1638 cm^{-1}) and results in the detection of a ν (Fe-CO) at 533 cm^{-1} (Figure 8), which is characteristic of heme-carbonyl complexes with a weak or no proximal ligand (24, 26–28).

NIH-PA Author Manuscript

NIH-PA Author Manuscript

NIH-PA Author Manuscript

Electrochemistry of Dap1p

Figure 9 shows the electrochemistry of wild-type Dap1p as evaluated using UV-Vis spectroelectrochemistry. The change in Soret band absorption upon reduction to ferrous heme was fit to an equilibrium midpoint reduction potential of −307 mV vs. SHE. This value is similar to the reduction potential of bovine catalase −260 mV vs. SHE value of bovine catalase, as well as other mono-tyrosinate heme proteins (29,30). Attempts to measure the reduction potential of *holo*-Dap1p^{Y138F} were thwarted by the extremely weak binding of ferrous heme to the mutant protein. However, since the reduction potential of a heme protein is determined by the relative stability of the ferric and ferrous heme states, the measured K_D values can be used to determine the reduction potential of the Dap1p^{Y138F} mutant (31). The 200 nM dissociation constant for ferric Dap1p^{Y138F} is 2000-fold weaker than the 400 pM value of ferric holo-Dap1p. Using the thermodynamic relationship, $\Delta G = -RT\ln K_{eq}$, the 2000-fold change in K_D represents a +4.5 kcal/mol destabilization of the ferric state Dap1p^{Y138F} relative to Dap1p. Since $\Delta E = \Delta\Delta G/nF$, the +4.5 kcal/mol destabilization of the ferric state should raise the midpoint potential +193 mV relative to Dap1p. The change in ferrous heme affinity also contributes to the reduction potential difference between these two proteins. The 5-fold, or 1 kcal/mol, destabilization of ferrous Dap1p^{Y138F} relative to Dap1p should lower the midpoint reduction potential of Dap1p^{Y138F} by 41 mV relative to Dap1p. Thus, the estimated reduction potential of Dap1p^{Y138F} is −155 mV, or −307 mV + 193 mV − 41 mV.

Discussion

As discussed in the introduction, there is an ongoing debate in the literature regarding the biological role of yeast Dap1p. It has been proposed that Dap1p is involved in stabilizing protein levels of the P_{450} enzyme, Erg11p, principally because deletion of Dap1p from the genome did not affect the RNA levels of Erg11p, but did affect both the Erg11p protein level and sterol synthesis (7). This hypothesis, however, was brought into question when Hughes et. al. observed that the protein levels of the human homologue of Erg11p (Cyp51A1) were unaffected by the absence of the human homologue of Dap1p (PGRMC1). Additionally, they reported a 1:1 stoichiometric protein-protein interaction between Dap1p and Erg11p, and found that *dap1Δ* cells transformed with the low affinity heme binding mutant, Dap1p^{Y138F}, also showed lowered sterol synthesis, suggesting that heme binding was critical for the ability of Dap1p to rescue sterol synthesis (8).

In order to probe the role of heme binding and Dap1p function further, we embarked on a more detailed investigation of Dap1p. Initially, we probed the cellular properties of Erg11p and observed no change in mRNA, or protein levels in the absence of genomic DAP1, consistent with the data of Hughes et. al. for the human homologues (8). In addition, we observed that the $t_{1/2}$ of Erg11p degradation was unchanged in *dap1Δ* strains. These results indicate that Dap1p does not stabilize Erg11p and weakens the case for Dap1p being a direct heme chaperone to Erg11p, as previously suggested (5–7).

Nevertheless, heme binding to Dap1p still appears to be required for ergosterol biosynthesis activity(8) and yet we previously reported that Dap1p, as isolated, only contained ~30% bound heme (6). We resolved this inconsistency in the current investigation by achieving 80 ± 20% heme loading for Dap1p with direct titration of free heme. This result indicated a tight affinity of the Dap1p for heme, however, the determination of the heme affinity to Dap1p (K_D) was unsuccessful by direct titration due to its tight K_D. HSM apo-myoglobin was then titrated into Dap1p (30% heme loaded) as a competitive substrate, and the K_D was approximated to be ~0.1 pM by singular value decomposition (14). This method assumes that the K_D of HSM apo-myoglobin, which has not been directly reported, is comparable to that of sperm whale myoglobin, whose K_D is ~0.01 pM (16). Having narrowed down the K_D range, Dap1p was titrated with $[\Delta\ 7\text{-His}]_2$, a well characterized synthetic heme binding peptide (K_D of 160 pM),

NIH-PA Author Manuscript

NIH-PA Author Manuscript

NIH-PA Author Manuscript

and the K_D of Dap1p was determined to be 400 ± 200 pM, with a 1:1 heme/protein ratio. This K_D value is significantly smaller than that expected for a non-specific hydrophobic pocket and supports the hypothesis that Dap1p is a heme binding protein (32). The ferrous heme affinity of Dap1p (K_D = 2 ± 1 μM), however, is significantly weaker than that of ferric heme, which is consistent with expectations based on hard-soft acid-base theory for charged tyrosinate as the axial ligand (33). Our RR data on the ferrous-carbonyl complex supports this conclusion. Axial ligands compete for σ-bond donation to the iron, and the high ν(Fe-CO) frequency observed in Dap1p is indicative of a weak trans ligand.

The reduction potential of Dap1p was measured to be −307 mV vs. SHE which is comparable to the −260 mV value of bovine catalase, whose axial ligand is also a tyrosinate (29,30). This value is in the range of cytochrome P_{450} reductases,(34) making it tempting to suggest that Dap1p could provide electrons to Erg11p and hence increase the Erg11p activity in the cell with Dap1p present, as suggested by Hughes et al. (8). However, this hypothesis is unlikely since typical electron transport proteins, such as cytochrome b5, have similar coordination environments between their biologically relevant oxidation states (35). In addition, since the ferrous heme does not bind well to Dap1p, the heme would likely dissociate during redox catalysis (35). Finally, attempts to reduce the rat Dap1p homologue, IZA, by P_{450} reductases and cytochrome b_5 have been unsuccessful *in vitro* (9).

Previously, we proposed that Y138 was the axial ligand based on the fact that the as-isolated phenylalanine mutant, $Dap1p^{Y138F}$ had no heme bound. We have subsequently been able to directly titrate $Dap1p^{Y138F}$ with free heme and have observed a 1:1 ratio of protein to heme, with a K_D of 200 ±100 nM. This affinity for heme is over 1000-fold weaker than that of Dap1p and is consistent with the loss of the native axial ligand, Y138 (32). The electronic spectrum of $Dap1p^{Y138F}$ with heme bound, however, is remarkably similar to that of Dap1p. This result possibly indicates either a loosely coordinated solvent molecule or an amino acid as a substitute axial ligand. The latter hypothesis is possible since there are a number of potential anionic ligands in close proximity within the hydrophobic pocket, as seen in the NMR structure of the non-heme bound, homologue At2g24940.1 (19). Interestingly, the K_D for $Dap1p^{Y138F}$ with ferrous heme is comparable to that of Dap1p (K_D = 10 μM), supporting the hypothesis that the ferrous heme iron is not coordinated to a strong axial ligand and that the hydrophobic pocket is the primary determinant for ferrous heme binding for both wild-type Dap1p and $Dap1p^{Y138F}$.

The fact that $Dap1p^{Y138F}$ still binds ferric heme with a relatively strong affinity inspired us to investigate the functional activity of this mutant protein. Hughes et al. demonstrated that $Dap1p^{Y138F}$ lowered sterol synthesis in yeast similar to that of the *dap1Δ* strain, supporting the necessity of heme binding to Dap1p for Erg11p activation. They did not, however, demonstrate if $Dap1p^{Y138F}$ could rescue the growth sensitivity of *dap1Δ* in the presence of MMS or fluconazole. We therefore expressed $Dap1p^{Y138F}$ under the endogenous promoter, in a *dap1Δ* strain, and found that $Dap1p^{Y138F}$ did indeed rescue both phenotypes. This was a perplexing result because the data of Hughes et al. showed that ergosterol biosynthesis with the $Dap1p^{Y138F}$ mutant is much lower than wild-type (8). However, the data also indicated that the total amount of ergosterol was still greater in $Dap1p^{Y138F}$ than in *dap1Δ* and more importantly, the level of the toxic dienol (ergosta-5,7-dienol) was lower in the $Dap1p^{Y138F}$ strain than in the *dap1Δ* strain. Since it is unclear what ratio of ergosterol to dienol is required to manifest the MMS and fluconazole sensitivity, we hypothesize that the lowered heme binding of $Dap1p^{Y138F}$ is still sufficient for a low level of activity which rescues the growth phenotypes, but not enough to match the sterol synthesis of wild-type Dap1p, as measured by GC-MS (8). This result supports the hypothesis that the heme binding is required for function and the biological activity Dap1p is regulated by its ability to bind heme. It should also be noted that we performed the growth sensitivity experiment with $Dap1p^{D91G}$ and found no

NIH-PA Author Manuscript

NIH-PA Author Manuscript

NIH-PA Author Manuscript

rescue, similar to that seen by Mallory and coworkers (7). The result is most likely due to the fact that Dap1p^{D91G} has an unstable protein structure, since we found no soluble Dap1p^{D91G} when it is expressed in *E. coli*.

The importance of heme binding for Dap1p appears in conflict with published data suggesting that MAPR's bind sterols (1,3,19,36,37). Reports of progesterone binding are predominantly with the porcine homologue PGRMC1, which was measured to have two binding affinities to progesterone, 11 nM and 286 nM (1). There is additional evidence for regulation of rat PGRMC1 (also known as Vema, IZA, 25-Dx, and sometimes mPR) by progesterone and involvement of PGRMC1 in cellular, non-genomic progesterone responses (37–42). However, progesterone binding by rat PGRMC1, was later shown to be nonspecific and weak by Min et al (5). Instead, they found that rat PGRMC1 bound heme and activated the cytochrome P_{450}, CYP21, a key enzyme of progesterone biosynthesis, similar to the biological function proposed by Hughes et al (8). These data indicate that MAPR's do bind heme and interact with P_{450} enzymes, but it may also be possible that they have a dual function and bind sterols as well, possibly competitively with heme. Clearly more studies are needed to clarify the full biological role of MAPR proteins.

In summary, we have made several interesting contributions towards characterizing Dap1p's role as a heme binding protein. First, we have demonstrated that Dap1p does not directly regulate the Erg11p at any level, be it mRNA, protein, or protein degradation. Secondly, Dap1p preferentially binds ferric heme tightly at a 1:1 stoichiometry (K_D = 400 pM) but ferrous heme poorly (K_D = 2 μM), supporting its designation as a ferric hemoprotein. Thirdly, the RR results and the reduction potential of Dap1p are consistent with a 5-coordinate heme iron with tyrosinate axial ligation (E = −307 mV). Finally, even though the weaker affinity of Dap1p^{Y138F} for ferric heme (K_D = 200 nM) lowers the production of ergosterol with respect to wild-type, it is still sufficient to rescue the growth sensitivity of *dap1Δ* to fluconazole and MMS, suggesting that the activity of Dap1p is directly related to its ability to bind heme and most likely not its redox potential.

Supplementary Material

Refer to Web version on PubMed Central for supplementary material.

Abbreviations

Dap1p, wild-type yeast Dap1 protein
Dap1p^{Y138F}, Dap1p-Tyr138fPhe
Dap1p^{D91G}, Dap1p-Asp91Gly
Erg11p, yeast Lanosterol 14-alpha-demethylase protein
Erg11p-HA, yeast Lanosterol 14-alpha-demethylase protein with a Hemagglutinin Tag on the C-Terminus
DAP1, wild-type yeast Dap1 gene
ERG11, yeast Lanosterol 14-alpha-demethylase gene
PGRMC1, progesterone receptor membrane component-1 protein
MAPR, membrane-associated progesterone binding protein
IZA, rat inner zone antigen
SD-His, synthetically defined media lacking histidine
PGK, phosphoglycerate kinase
AAA, amino acid analysis
ICP-MS, Inductively Coupled Plasma Mass Spectrometry
MMS, methyl methanesulfonate
Mb, myoglobin

NIH-PA Author Manuscript

NIH-PA Author Manuscript

NIH-PA Author Manuscript

apoMb, apomyoglobin
HSM, horse skeletal muscle
TBP, TATA box binding protein
RR, Resonance Raman
SHE, standard hydrogen electrode
GC-MS, gas chromatography mass spectrometry

Acknowledgement

We would like to thank Zhu Zhiwu and Chris Vulpe for valuable discussions.

References

1. Meyer C, Schmid R, Scriba PC, Wehling M. Purification and partial sequencing of high-affinity progesterone-binding site(s) from porcine liver membranes. Eur J Biochem 1996;239:726–731. [PubMed: 8774719]
2. Falkenstein E, Meyer C, Eisen C, Scriba PC, Wehling M. Full-length cDNA sequence of a progesterone membrane-binding protein from porcine vascular smooth muscle cells. Biochem Biophys Res Commun 1996;229:86–89. [PubMed: 8954087]
3. Falkenstein E, Eisen C, Schmieding K, Krautkramer M, Stein C, Losel R, Wehling M. Chemical modification and structural analysis of the progesterone membrane binding protein from porcine liver membranes. Mol Cell Biochem 2001;218:71–79. [PubMed: 11330840]
4. Mifsud W, Bateman A. Membrane-bound progesterone receptors contain a cytochrome b5-like ligand-binding domain. Genome Biol 2002;3:1–5.
5. Min L, Strushkevich NV, Harnastai IN, Iwamoto H, Gilep AA, Takemori H, Usanov SA, Nonaka Y, Hori H, Vinson GP, Okamoto M. Molecular identification of adrenal inner zone antigen as a heme-binding protein. Febs J 2005;272:5832–5843. [PubMed: 16279947]
6. Ghosh K, Thompson AM, Goldbeck RA, Shi X, Whitman S, Oh E, Zhiwu Z, Vulpe C, Holman TR. Spectroscopic and Biochemical Characterization of Heme Binding to Yeast Dap1p and Mouse PGRMC1p. Biochemistry 2005;44:16729–16736. [PubMed: 16342963]
7. Mallory JC, Crudden G, Johnson BL, Mo C, Pierson CA, Bard M, Craven RJ. Dap1p, a heme-binding protein that regulates the cytochrome P450 protein Erg11p/Cyp51p in Saccharomyces cerevisiae. Mol Cell Biol 2005;25:1669–1679. [PubMed: 15713626]
8. Hughes AL, Powell DW, Bard M, Eckstein J, Barbuch R, Link AJ, Espenshade PJ. Dap1/PGRMC1 binds and regulates cytochrome P450 enzymes. Cell Metab 2007;5:143–149. [PubMed: 17276356]
9. Min L, Takemori H, Nonaka Y, Katoh Y, Doi J, Horike N, Osamu H, Raza FS, Vinson GP, Okamoto M. Characterization of the adrenal-specific antigen IZA (inner zone antigen) and its role in the steroidogenesis. Mol Cell Endocrinol 2004;215:143–148. [PubMed: 15026187]
10. Hand RA, Jia N, Bard M, Craven RJ. Saccharomyces cerevisiae Dap1p, a novel DNA damage response protein related to the mammalian membrane-associated progesterone receptor. Eukaryot Cell 2003;2:306–317. [PubMed: 12684380]
11. Ooi CE, Rabinovich E, Dancis A, Bonifacino JS, Klausner RD. Copper-dependent degradation of the Saccharomyces cerevisiae plasma membrane copper transporter Ctr1p in the apparent absence of endocytosis. Embo J 1996;15:3515–3523. [PubMed: 8670854]
12. Padmanabhan S, Marqusee S, Ridgeway T, Laue TM, Baldwin RL. Relative helix-forming tendencies of nonpolar amino acids. Nature 1990;344:268–270. [PubMed: 2314462]
13. Berry EA, Trumpower BL. Simultaneous determination of hemes a, b, and c from pyridine hemochrome spectra. Anal Biochem 1987;161:1–15. [PubMed: 3578775]
14. Hendler RW, Shrager RI. Deconvolutions based on singular value decomposition and the pseudoinverse: a guide for beginners. J Biochem Biophys Methods 1994;28:1–33. [PubMed: 8151067]
15. Hargrove MS, Olson JS. The stability of holomyoglobin is determined by heme affinity. Biochemistry 1996;35:11310–11318. [PubMed: 8784185]

NIH-PA Author Manuscript

NIH-PA Author Manuscript

NIH-PA Author Manuscript

16. Hargrove MS, Wilkinson AJ, Olson JS. Structural factors governing hemin dissociation from metmyoglobin. Biochemistry 1996;35:11300–11309. [PubMed: 8784184]
17. Reddi AR, Reedy CJ, Mui S, Gibney BR. Thermodynamic investigation into the mechanisms of proton-coupled electron transfer events in heme protein maquettes. Biochemistry 2007;46:291–305. [PubMed: 17198400]
18. Dutton PL. Redox potentiometry: determination of midpoint potentials of oxidation-reduction components of biological electron-transfer systems. Methods Enzymol 1978;54:411–435. [PubMed: 732578]
19. Song J, Vinarov D, Tyler EM, Shahan MN, Tyler RC, Markley JL. Hypothetical protein At2g24940.1 from Arabidopsis thaliana has a cytochrome b5 like fold. J Biomol NMR 2004;30:215–218. [PubMed: 15702529]
20. Fronticelli C, Bucci E. Acetone Extraction Of Heme From Myoglobin And Hemoglobin At Acid Ph. Biochim Biophys Acta 1963;78:530–531. [PubMed: 14088783]
21. Teale FWJ. Cleavage of the haem-protein link by acid methylethylketone. Biochimica et Biophysica Acta 1959;35:543. [PubMed: 13837237]
22. Reedy CJ, Kennedy ML, Gibney BR. Thermodynamic characterization of ferric and ferrous haem binding to a designed four-alpha-helix protein. Chem Commun (Camb) 2003:570–571. [PubMed: 12669829]
23. Spiro, TGL,X-Y. Biological Applications of Raman Spectroscopy. Vol. Vol. 3. New York: John Wiley & Sons; 1988. Resonance Raman Spectroscopy of Metalloporphyrins.
24. Liu Y, Moenne-Loccoz P, Hildebrand DP, Wilks A, Loehr TM, Mauk AG, Ortiz de Montellano PR. Replacement of the proximal histidine iron ligand by a cysteine or tyrosine converts heme oxygenase to an oxidase. Biochemistry 1999;38:3733–3743. [PubMed: 10090762]
25. Eakanunkul S, Lukat-Rodgers GS, Sumithran S, Ghosh A, Rodgers KR, Dawson JH, Wilks A. Characterization of the periplasmic heme-binding protein shut from the heme uptake system of Shigella dysenteriae. Biochemistry 2005;44:13179–13191. [PubMed: 16185086]
26. Sun J, Loehr TM, Wilks A, Ortiz de Montellano PR. Identification of histidine 25 as the heme ligand in human liver heme oxygenase. Biochemistry 1994;33:13734–13740. [PubMed: 7947784]
27. Franzen S, Bailey J, Dyer RB, Woodruff WH, Hu RB, Thomas MR, Boxer SG. A photolysis-triggered heme ligand switch in H93G myoglobin. Biochemistry 2001;40:5299–5305. [PubMed: 11318654]
28. Ray GB, Li X-Y, Ibers JA, Sessler JL, Spiro TG. How far can proteins bend the FeCO unit? Distal polar and steric effects in heme proteins and models. J Am Chem Soc 1994;116:162–176.
29. Wang L, Wang J, Zhou F. Direct electrochemistry of catalase at a gold electrode modified with single-wall carbon nanotubes. Electroanalysis 2004;16:627–632.
30. Hildebrand DP, Burk DL, Maurus R, Ferrer JC, Brayer GD, Mauk AG. The proximal ligand variant His93Tyr of horse heart myoglobin. Biochemistry 1995;34:1997–2005. [PubMed: 7849057]
31. Reedy CJ, Gibney BR. Heme protein assemblies. Chem Rev 2004;104:617–649. [PubMed: 14871137]
32. Hargrove MS, Barrick D, Olson JS. The association rate constant for heme binding to globin is independent of protein structure. Biochemistry 1996;35:11293–11299. [PubMed: 8784183]
33. Pearson RG. Hard and Soft Acids and Bases. J Am Chem Soc 1963;85:3533–3539.
34. Munro AW, Noble MA, Robledo L, Daff SN, Chapman SK. Determination of the redox properties of human NADPH-cytochrome P450 reductase. Biochemistry 2001;40:1956–1963. [PubMed: 11329262]
35. Gray HB, Winkler JR. Electron tunneling through proteins. Quarterly Rev Biophys 2004;36:341–372.
36. Losel R, Dorn-Beineke A, Falkenstein E, Wehling M, Feuring M. Porcine spermatozoa contain more than one membrane progesterone receptor. Int J Biochem Cell Biol 2004;36:1532–1541. [PubMed: 15147732]
37. Falkenstein E, Heck M, Gerdes D, Grube D, Christ M, Weigel M, Buddhikot M, Meizel S, Wehling M. Specific progesterone binding to a membrane protein and related nongenomic effects on Ca2+-fluxes in sperm. Endocrinology 1999;140:5999–6002. [PubMed: 10579369]

NIH-PA Author Manuscript

NIH-PA Author Manuscript

NIH-PA Author Manuscript

38. Labombarda F, Gonzalez SL, Deniselle MC, Vinson GP, Schumacher M, De Nicola AF, Guennoun R. Effects of injury and progesterone treatment on progesterone receptor and progesterone binding protein 25-Dx expression in the rat spinal cord. J Neurochem 2003;87:902–913. [PubMed: 14622121]

39. Peluso JJ. Non-genomic actions of progesterone in the normal and neoplastic mammalian ovary. Semin Reprod Med 2007;25:198–207. [PubMed: 17447209]

40. Peluso JJ, Pappalardo A, Losel R, Wehling M. Progesterone membrane receptor component 1 expression in the immature rat ovary and its role in mediating progesterone's antiapoptotic action. Endocrinology 2006;147:3133–3140. [PubMed: 16513825]

41. Gonzalez SL, Labombarda F, Deniselle MC, Mougel A, Guennoun R, Schumacher M, De Nicola AF. Progesterone neuroprotection in spinal cord trauma involves up-regulation of brain-derived neurotrophic factor in motoneurons. J Steroid Biochem Mol Biol 2005;94:143–149. [PubMed: 15862959]

42. Krebs CJ, Jarvis ED, Chan J, Lydon JP, Ogawa S, Pfaff DW. A membrane-associated progesterone-binding protein, 25-Dx, is regulated by progesterone in brain regions involved in female reproductive behaviors. Proc Natl Acad Sci U S A 2000;97:12816–12821. [PubMed: 11070092]

NIH-PA Author Manuscript

NIH-PA Author Manuscript

NIH-PA Author Manuscript

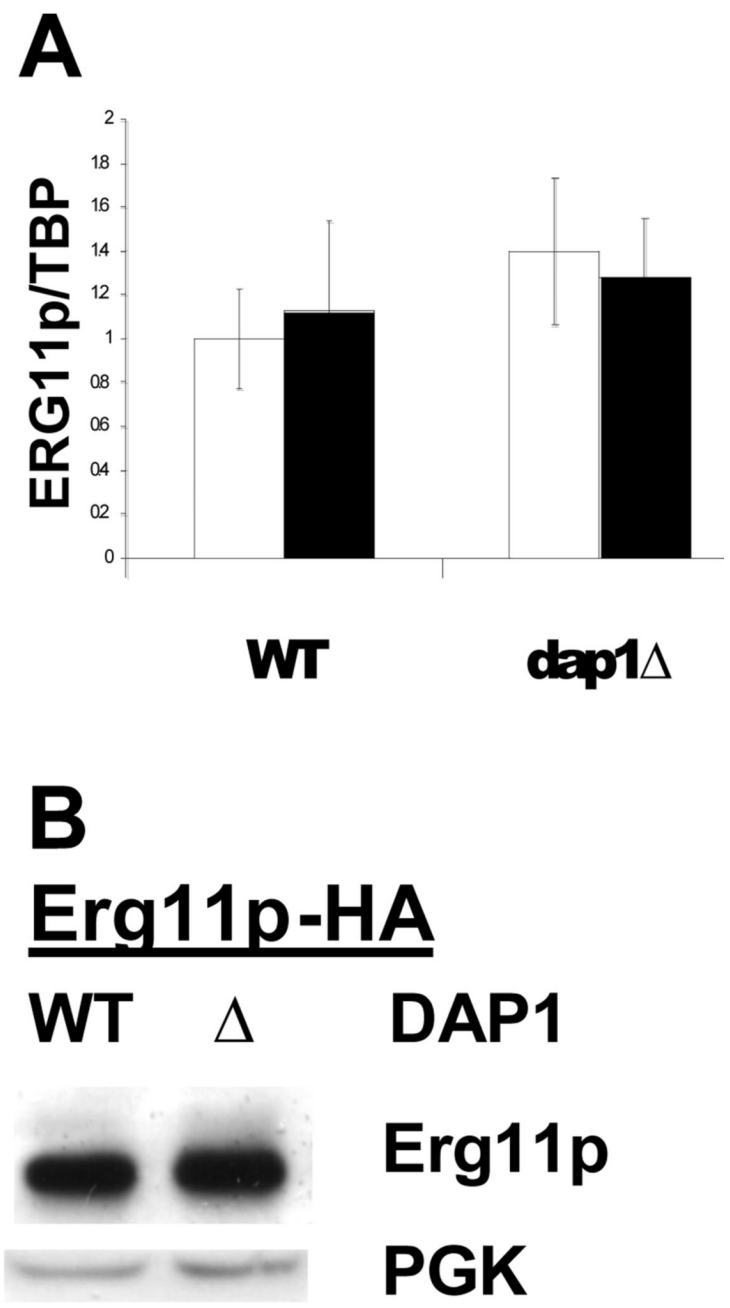

Figure 1.
Wild-type and *dap1Δ* yeast strains were tested for A) DNA expression levels of ERG11, as measured by rtPCR (normalized to TBP), while grown with heme (black) and without heme (white) and B) Protein expression levels measured by western blot, without heme added.

NIH-PA Author Manuscript

NIH-PA Author Manuscript

NIH-PA Author Manuscript

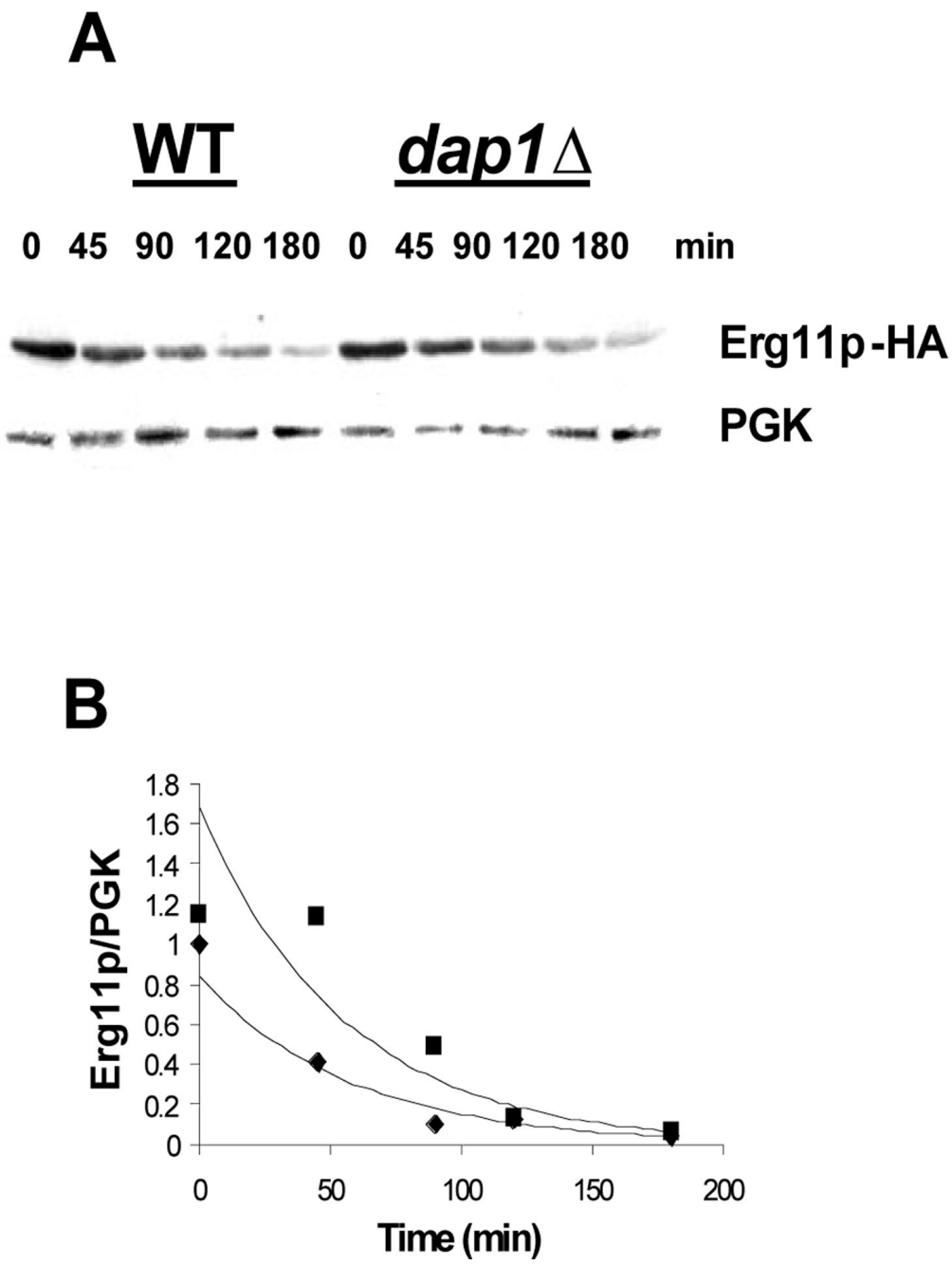

Figure 2.

Measurement of $t_{1/2}$ of Erg11 p in wild-type and *dap1Δ* yeast strains. A) Protein expression levels of Erg11p and PGK at 0, 45, 90, 120, and 180 mins after repression by glucose of Erg11 p-HA on the galactose promoter. B) Calculation of Erg11 p degradation rates, relative to PGK (♦) $t_{1/2}$ = 40 mins and *dap1Δ* (▪) $t_{1/2}$ = 38.

NIH-PA Author Manuscript

NIH-PA Author Manuscript

NIH-PA Author Manuscript

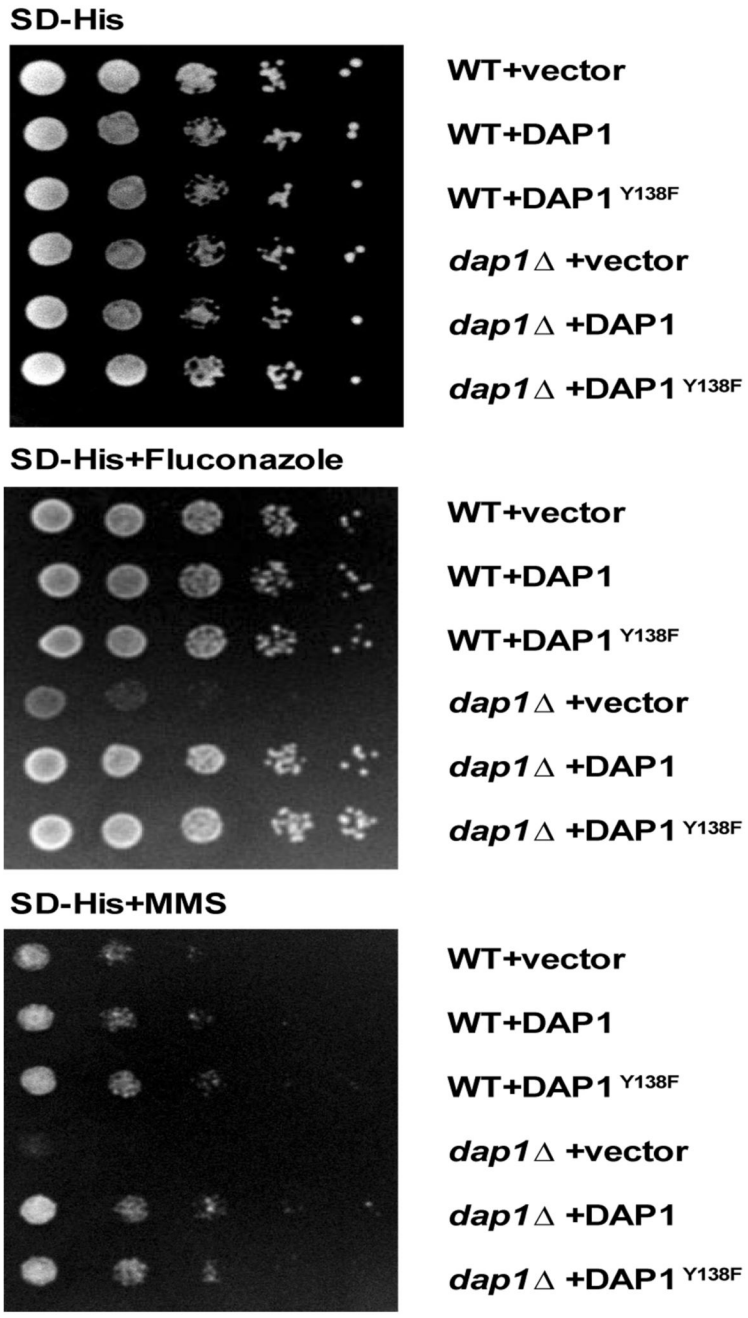

Figure 3.
Growth of yeast strains wild-type (BY4741) or isogenic *dap1Δ* transformed with pRS313 vector containing either vector only, DAP1, or DAP1^{Y138F}. Cells were serial diluted 1:10 and grown for 3 days at 30°C.

NIH-PA Author Manuscript

NIH-PA Author Manuscript

NIH-PA Author Manuscript

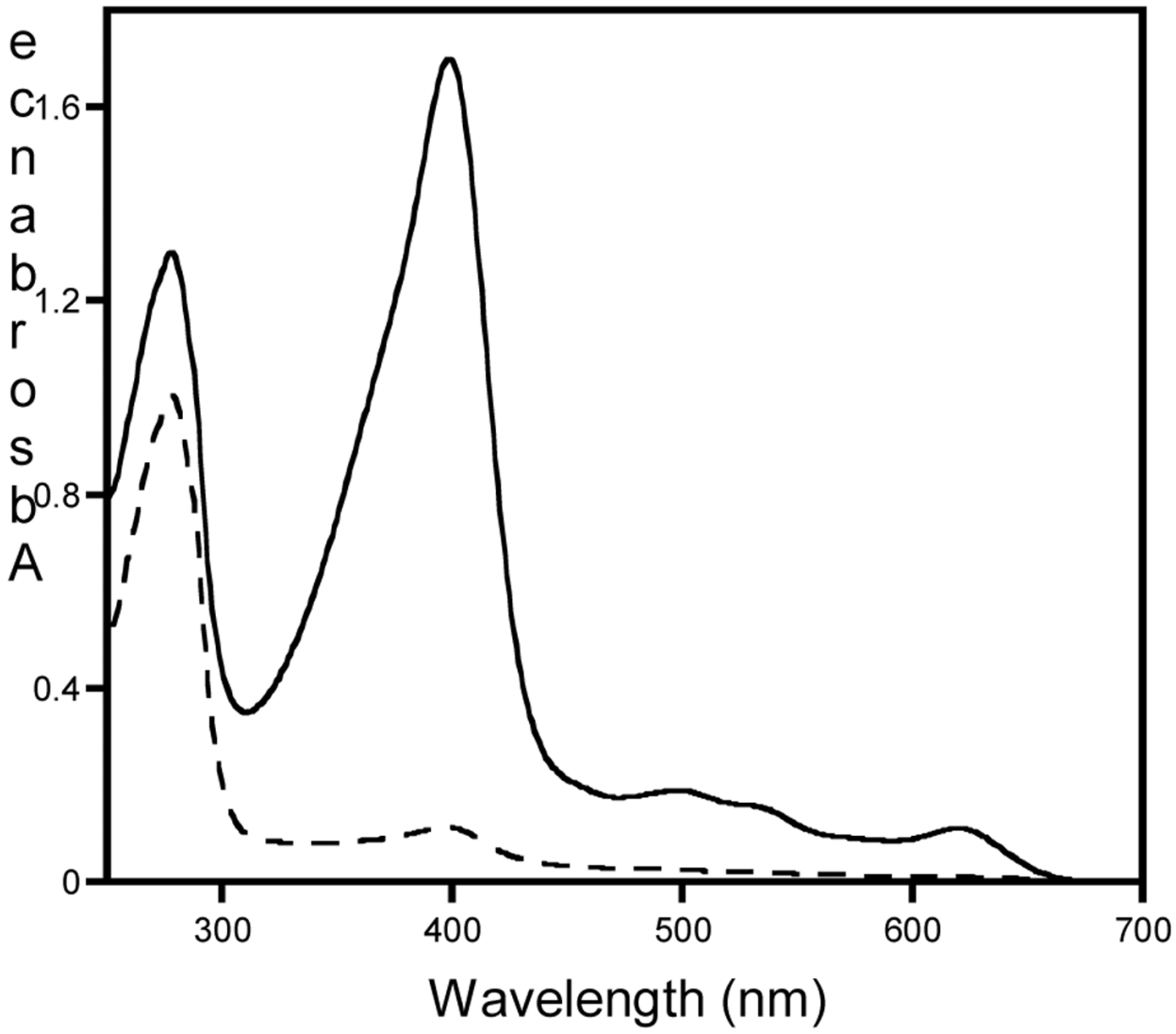

Figure 4.
Representative UV-visible spectra of 1 mg/ml samples Dap1p (—) (as purified with ~20% heme bound) and Dap1p^{Y138F} (--) (as purified with <2% heme bound).

NIH-PA Author Manuscript
NIH-PA Author Manuscript
NIH-PA Author Manuscript

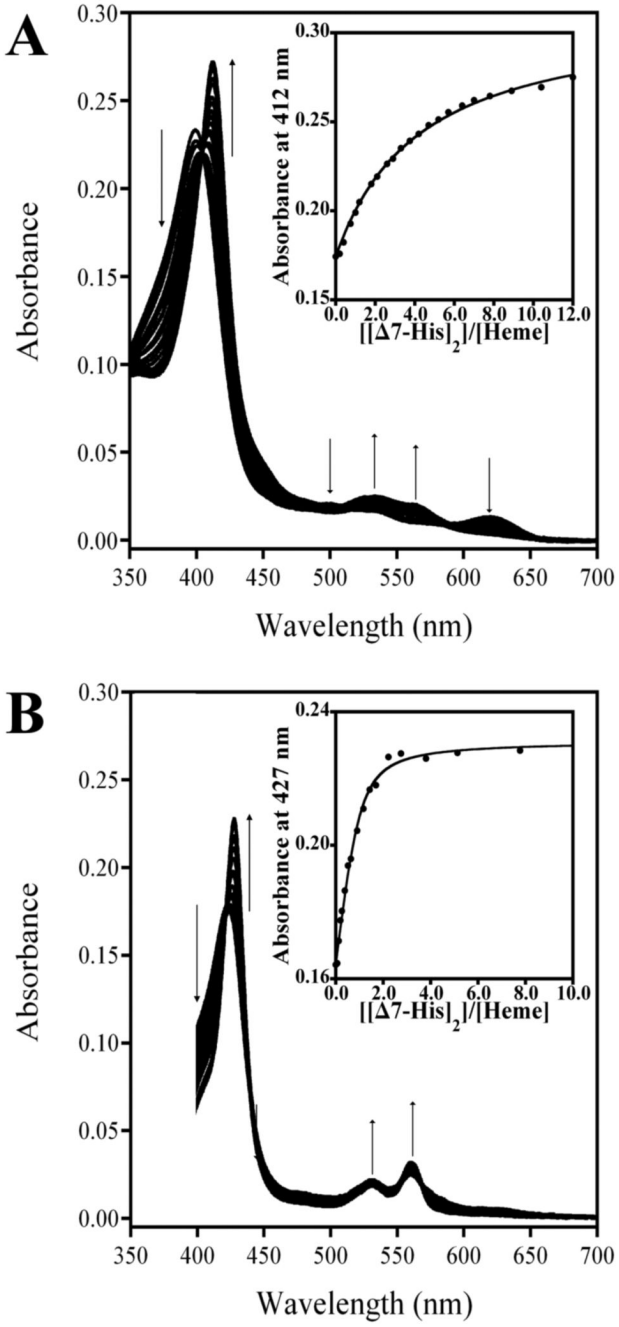

Figure 5.

Representative competition titration of ferric (A) and ferrous (B) heme loaded Dap1p with $[\Delta 7\text{-His}]_2$. The insets, which show the increase in absorption at the Soret of heme loaded $[\Delta\text{-His}]_2$, indicate the transfer of heme from Dap1p to $[\Delta 7\text{-His}]_2$; the change in absorption is fit to a competition model that gives the ferric and ferrous heme loaded Dap1 p K_D values.

NIH-PA Author Manuscript
NIH-PA Author Manuscript
NIH-PA Author Manuscript

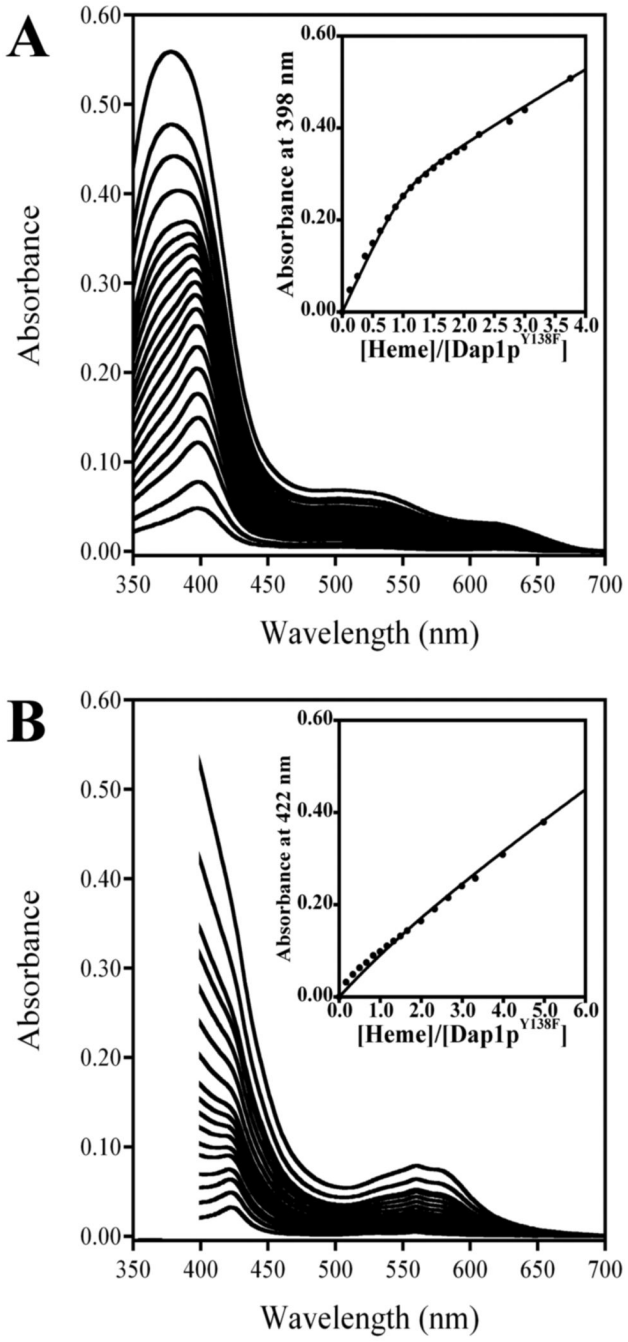

Figure 6.

Direct titration of ferric (A) and ferrous (B) heme into Dap1p^{Y138F}. Insets show the change in absorption at the Soret as a result of heme binding, and are fit to 1:1 binding models that give the ferric and ferrous K_D values of Dap1p^{Y138F}.

NIH-PA Author Manuscript
NIH-PA Author Manuscript
NIH-PA Author Manuscript

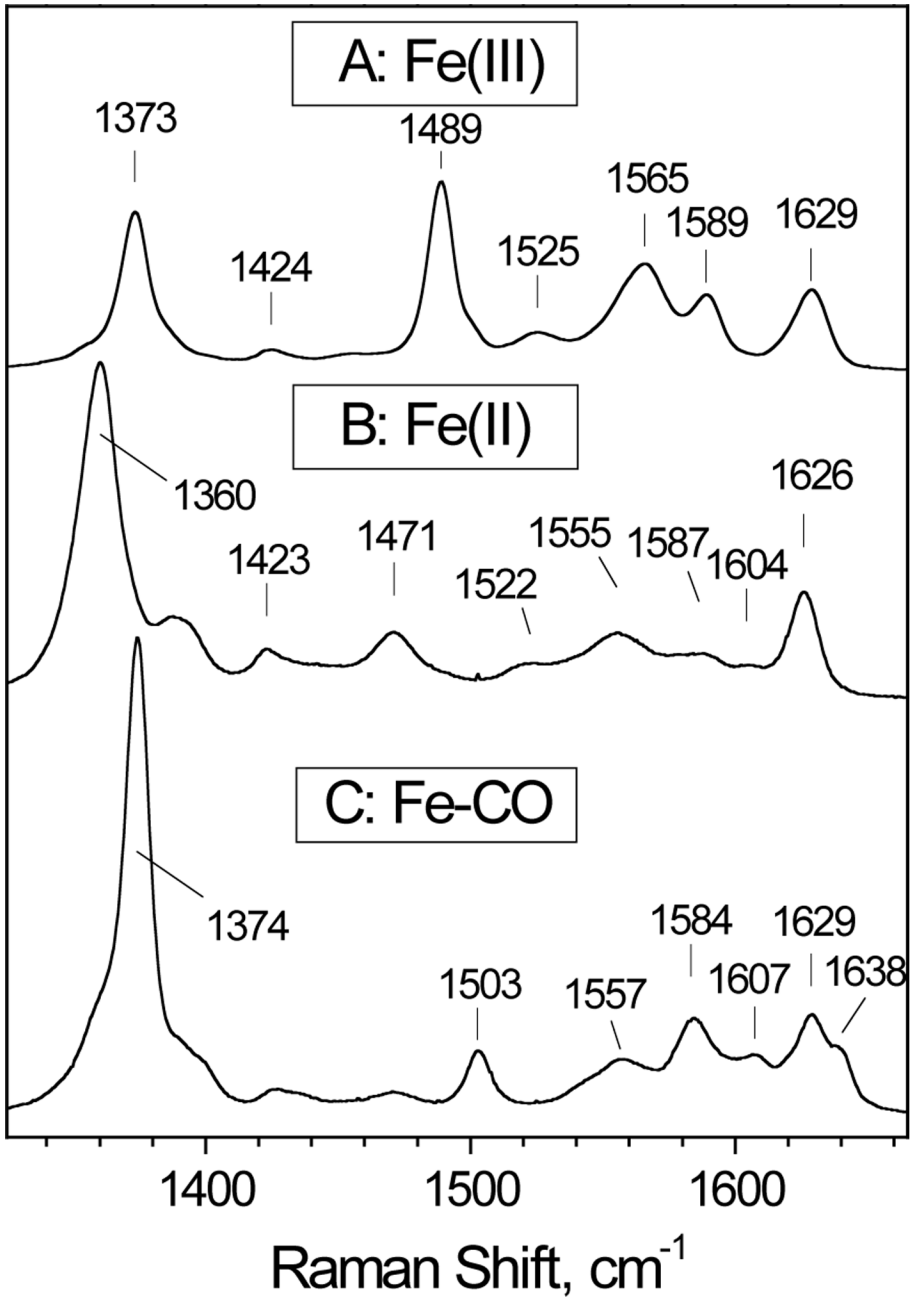

Figure 7.
High-frequency region of the RR spectra of Dap1p ferric (A), ferrous (B), and ferrous-CO complex (C) obtained at room temperature with a 413-nm excitation.

NIH-PA Author Manuscript
NIH-PA Author Manuscript
NIH-PA Author Manuscript

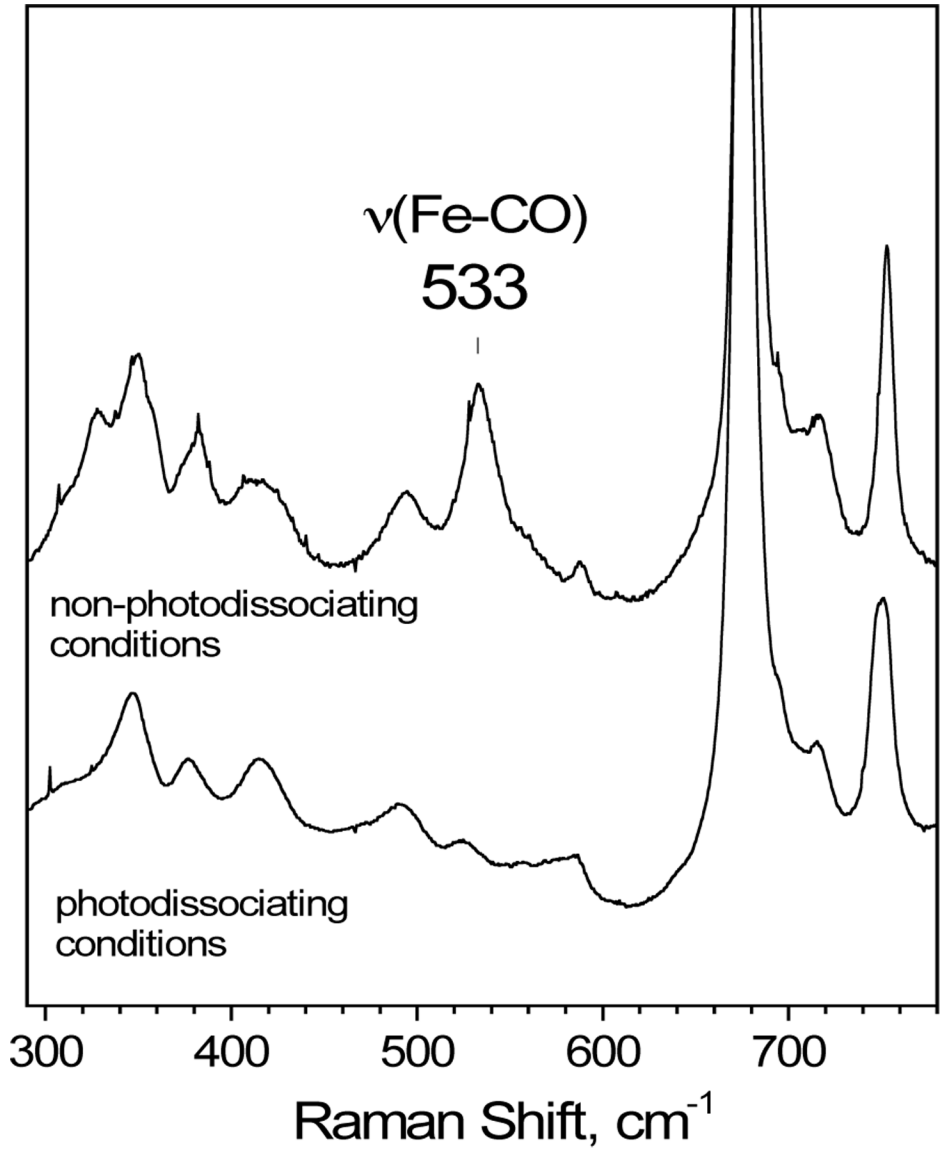

Figure 8.
Low-frequency region of the RR spectra of the ferrous-CO complex of Dap1p obtained at room temperature with a 413-nm excitation. To achieve non-photodissociating conditions, the laser beam was defocused on the samples and kept below less than 1 mW using neutral density filter.

NIH-PA Author Manuscript

NIH-PA Author Manuscript

NIH-PA Author Manuscript

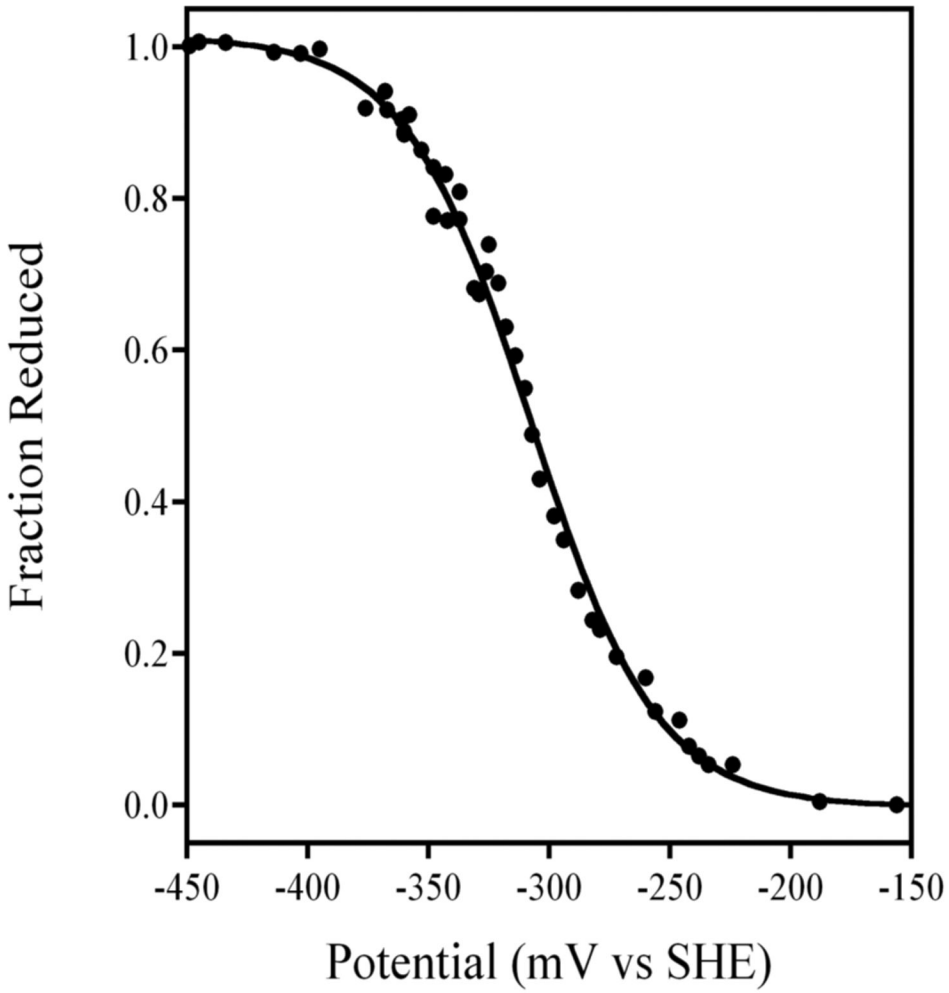

Figure 9.
Redox potentiometry of heme loaded Dap1p. The change in absorbance at the Soret as a function of solution potential is best fit to an $n = 1$ Nernst equation that gives a reduction potential of −307 mV vs. SHE.